

# PROCEEDINGS OF SPIE

[SPIDigitalLibrary.org/conference-proceedings-of-spie](https://spiedigitallibrary.org/conference-proceedings-of-spie)

## Production of 8.4 m primary mirror segments for GMT

H. M. Martin, R. Ceragioli, V. Gasho, B. T. Jannuzi, D. W. Kim, et al.

H. M. Martin, R. Ceragioli, V. Gasho, B. T. Jannuzi, D. W. Kim, J. S. Kingsley, K. Law, A. Loeff, R. D. Lutz, S. Meyen, C. J. Oh, M. T. Tuell, S. N. Weinberger, S. C. West, R. Whitsitt, R. Wortley, "Production of 8.4 m primary mirror segments for GMT," Proc. SPIE 12188, Advances in Optical and Mechanical Technologies for Telescopes and Instrumentation V, 121880J (20 September 2022); doi: 10.1117/12.2630378

**SPIE.**

Event: SPIE Astronomical Telescopes + Instrumentation, 2022, Montréal, Québec, Canada

# Production of 8.4 m primary mirror segments for GMT

H. M. Martin<sup>a</sup>, R. Ceragioli<sup>a</sup>, V. Gasho<sup>a</sup>, B. T. Januzzi<sup>a</sup>, D. W. Kim<sup>b</sup>, J. S. Kingsley<sup>a</sup>, K. Law<sup>a</sup>, A. Loeff<sup>a</sup>, R. D. Lutz<sup>a</sup>, S. Meyen<sup>a</sup>, C. J. Oh<sup>b</sup>, M. T. Tuell<sup>a</sup>, S. N. Weinberger<sup>a</sup>, S. C. West<sup>a</sup>, R. Whitsitt<sup>a</sup> and R. Wortley<sup>a</sup>

<sup>a</sup>Steward Observatory, University of Arizona, Tucson, AZ 85721, USA

<sup>b</sup>College of Optical Sciences, University of Arizona, Tucson, AZ 85721, USA

## ABSTRACT

The Richard F. Caris Mirror Lab at the University of Arizona continues production of 8.4 m lightweight honeycomb segments for the primary mirror of the Giant Magellan Telescope. GMT's 25 m primary mirror consists of a center segment surrounded by six off-axis segments, with an additional off-axis segment to allow continuous operation as segments are removed for coating. We cast the sixth segment (5 off-axis segments + center segment) in March 2021. As of June 2022 we have tentatively completed polishing of the third off-axis segment, and we are in the process of grinding the optical surface of off-axis Segment 5. For Segment 3, we improved the measurement accuracy for small-scale structure near the edge of the mirror, which has been a challenge for the off-axis segments. In addition to full-aperture interferometry and deflectometry, we used a 20 cm test plate to obtain high-resolution interferometric measurements of the edge.

**Keywords:** Giant Magellan Telescope, telescopes, optical fabrication, optical testing, off-axis, aspheres

## 1. INTRODUCTION

GMT<sup>[1],[2]</sup>, one of the new generation of extremely large telescopes, has a 25 m primary mirror comprising seven 8.4 m lightweight honeycomb mirrors. These segments are the stiffest and lightest large mirrors ever made and therefore minimize deflections due to gravity and wind. The use of 8.4 m segments guarantees a smooth wavefront over large fractions of the aperture. Each primary segment is paired with a 1.1 m segment of the adaptive secondary mirror; fine alignment and phasing are achieved with the agile secondary segments. The primary mirror segments are being made at the Richard F. Caris Mirror Lab at the University of Arizona. Off-axis segments 1 and 2 are finished, Segment 3 is finished pending acceptance, and Segments 4-6 are in different stages of manufacture. Segments are numbered in order of casting; Segment 4 is the center segment.

The six off-axis segments have strong, non-axisymmetric asphericity and present significant challenges in fabrication and testing. A set of independent optical tests measures the mirror figure on scales from 8.4 m down to 1 cm.<sup>[4]-[8]</sup> The overlapping capabilities of the tests provide redundant measurements of critical parameters, in particular the radius of curvature and low-order aberrations. Multiple sets of measurements on Segments 1-3 have shown that the tests agree within the expected uncertainties.<sup>[3]</sup> The full-aperture tests work well for measuring about 95% of the surface, but the outer 10 cm generally has enough small-scale structure to cause some loss of data and erroneous data. We have obtained accurate information by measuring the edge with a 20 cm spherical test plate (using interference between the segment surface and the test plate), giving spatial resolution of 1-5 mm depending on fringe density. For Segment 3 we refined this method to make it safer and more efficient, and we used it more extensively to guide figuring and to characterize the finished surface.

## 2. STATUS OF SEGMENT PRODUCTION

Highlights of the last two years include the tentative completion of Segment 3 (pending acceptance), progress on generating the optical surface of Segment 5, and spin-casting of Segment 6. Segments 1 and 2 are complete and in storage in Tucson. For Segment 4, the center segment, we have completed work on the rear surface, including bonding the 165 loadspreaders that form the interface between the mirror and its support system in the telescope. Optical testing of Segment 4 requires a reconfiguration of the test tower, and we plan to complete off-axis Segment 5 and possibly more off-axis segments before we figure the optical surface of Segment 4. We have nearly finished diamond generating the optical surface of Segment 5. The next section describes the spin-casting of Segment 6. We have purchased 20 tons of Ohara E6 low-expansion

borosilicate glass for Segment 7. We expect completion of all segments on a schedule consistent with the telescope project timeline.

### 3. SPIN-CASTING OF SEGMENT 6

We have described the spin-casting process in [9] and [10]. The 12-month process is condensed to a 6-minute video at <https://mirrorlab.arizona.edu/content/gmt-giant-magellan-telescope>. The spin-casting of Segment 6 went smoothly. Prior to the casting we carried out two upgrades to the furnace control system, installing new Linux-based control software and an all-digital rotation control system.

We melt the glass in a mold consisting of a tub of silicon carbide cement, wrapped with Inconel steel bands to support its cylindrical wall, and lined with ceramic fiber. For a GMT off-axis segment, the honeycomb mirror has 1681 cavities formed by ceramic fiber boxes (Figure 1). Each box is bolted to the floor of the mold with silicon carbide hardware and a ceramic fiber spacer to hold the box 30 mm above the floor. The ceramic fiber is made by Rex Materials and machined to final dimensions at the Mirror Lab. The ceramic fiber is the only material other than air that the glass contacts. Its strength is much less than that of glass and it does not interact chemically with the glass, so it can be separated from the glass safely after the casting. Viewed from above, most of the boxes are identical regular hexagons, but they have different heights and their tops are tilted to follow the optical surface so the finished mirror will have a uniform facesheet, 28 mm thick. This means all 1681 boxes are unique, although the shapes have mirror symmetry across an axis that runs through the center of the parent surface.

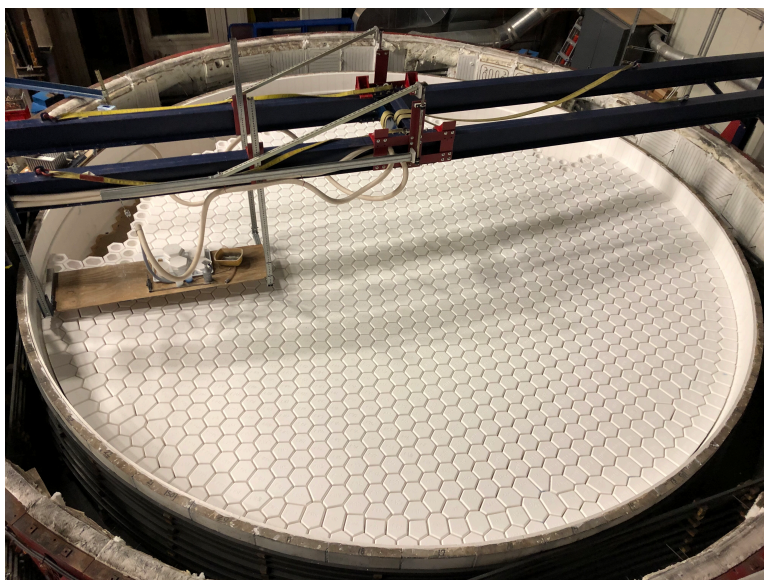


Figure 1. Nearly completed mold for casting GMT Segment 6.

For a GMT off-axis segment, we place 17,500 kg of Ohara E6 low-expansion borosilicate glass on top of the mold. Grinding will reduce the mass of the finished mirror to about 16,000 kg. Ohara makes the glass in one-ton clay pots and breaks each ton into blocks of 2-3 kg each for delivery to the Mirror Lab. The blocks have pristine fracture surfaces that melt together during the casting with no trace of the original blocks.

We applied heater power to the furnace on March 1, 2021 to cast Segment 6. The furnace started spinning at 4.9 rpm at a temperature of 750°C on March 5. The peak temperature of 1165°C was reached the next day, giving the glass a viscosity similar to molasses. Four hours at high temperature allows the glass to flow down 12 mm gaps between the hexagonal boxes and fill the mold. The mirror cooled quickly to 530°C, to begin 6 weeks of annealing at a cooling rate of 3 K/day, followed by a faster cool down to room temperature. We opened the furnace on June 7 to find a high-quality mirror blank shown in Figure 2, with all dimensions in tolerance.

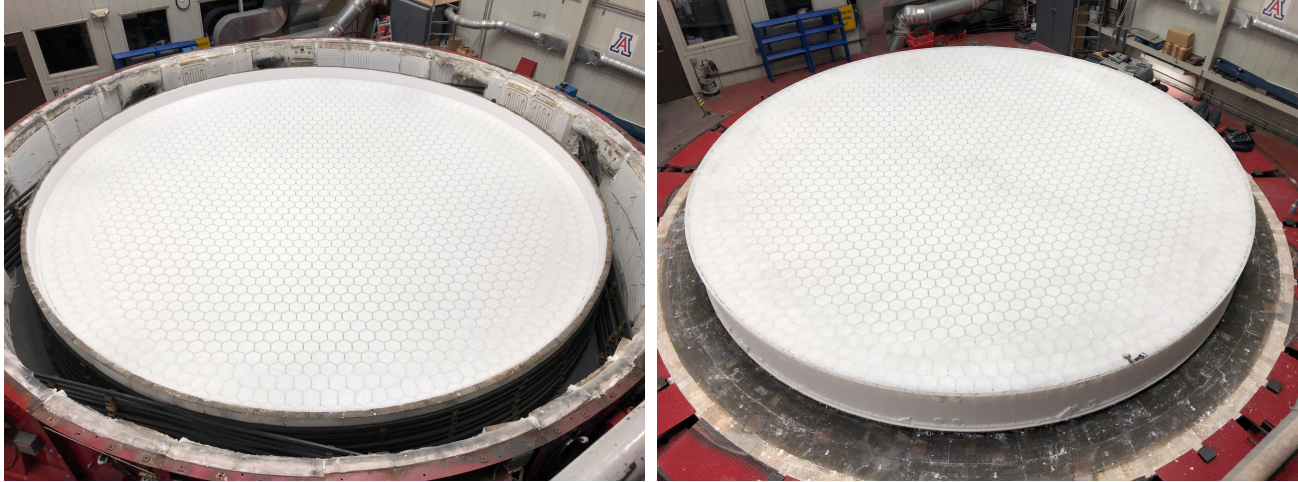


Figure 2. Cast mirror blank for GMT Segment 6, before and after removal of the furnace cylinder and the silicon carbide tub wall. At this point the ceramic fiber boxes are still in the honeycomb mirror and visible through the transparent glass.

The final step of the casting process was to remove the mold materials that were still attached to the mirror. We lifted the mirror and rotated it into a vertical plane, giving access to the rear surface. We first removed the silicon carbide floor tiles and bolts from the mirror's backplate. Each bolt and its ceramic fiber collar form a 90 mm hole in the backplate at the center of each honeycomb cell. We inserted high-pressure water nozzles through these holes to break up the ceramic fiber and wash it out of the mirror. (The same holes are used to ventilate the mirror in operation at the telescope.) Removal of the ceramic fiber left a lightweight glass structure with the desired mechanical and thermal properties. Once the mirror was clean and dry, a detailed inspection in October revealed no fractures or damage other than typical minor chips on a few of the 1681 ventilation holes.

The 4.9 rpm rotation creates a symmetric paraboloid with  $R = 37$  m that will require minimal removal to produce the off-axis optical surface with its 13 mm p-v asphericity. We form this surface and remove several millimeters of excess glass when we diamond generate the optical surface.

## 4. POLISHING OF SEGMENT 3

### 4.1 Polishing methods

We polished Segment 3 using essentially the same methods as for Segment 2: computer-controlled polishing with orbital motion using laps ranging from 40 cm to 4 cm in diameter. We control the figure by varying the dwell as a function of position on the mirror. The laps must accommodate large curvature variations over the off-axis mirror; the local radius of curvature varies from 36.3 m to 43.0 m and all points have significant astigmatism. The laps are designed so that plate flexure and pitch flow reduce their misfit relative to the aspheric surface. While the dominant motion is the lap's orbit, lap rotation is also controlled and generally used to keep the lap at a fixed orientation in parent coordinates, minimizing the necessary shape change due to local astigmatism of the off-axis surface. Figure 3 shows a 40 cm lap and a 10 cm lap used at different stages of polishing.

It is relatively easy to obtain a smooth and accurate surface over a large majority of the surface. The most challenging and time-consuming part of the process is controlling small-scale structure near the edge. For Segment 3 the last 4 polishing cycles included use of a 4 cm lap over the outer 10 cm of the surface, giving slow but steady improvement in each cycle.



Figure 3. GMT Segment 3 being polished with a 40 cm pitch lap at left and a 10 cm lap at right. Both laps are driven by the same orbital polisher.

#### 4.2 Use of a test plate to measure the edge

The segment's optical surface is 8.405 m in diameter and has a clear aperture of 8.365 m, i.e. the surface must meet its accuracy requirements to within 20 mm of the edge. The figure specification is in the form of a structure function, giving allowed error as a function of spatial scale, and emphasizes smoothness on scales  $< 5$  cm. Generally, the dominant small-scale structure is concentrated near the edge. It has a large impact on the structure function and on our ability to measure the surface with the full-aperture optical tests.

To guide polishing at the outer 10 cm of Segment 3, we measured small-scale structure using the interference between the mirror surface and a 20 cm spherical test plate. Profiles of the edge in the radial direction were measured every  $10^\circ$  in azimuth (or polar angle) on a routine basis. Although this is time-consuming and requires repeated mechanical contact between the test plate and the segment, we have refined the procedure over the course of its use on Segment 3 to minimize risk and improve efficiency. The radial profiles obtained with the test plate are by far the best measurement of structure in the outer 10 cm. The choice of  $10^\circ$  intervals in azimuth (0.7 m along the edge) is a compromise between increased information on the one hand and time and risk on the other. Structure near the edge varies rapidly in radius and much more slowly in azimuth, so relatively coarse sampling in azimuth gives a complete and accurate assessment of the surface.

The setup and acquisition of the measurement is illustrated in Figure 4. The test plate is carefully placed on the segment surface, overlapping the edge. Then, without moving the camera or the test plate, two images with the whole test plate in view are taken with a tripod-mounted camera. The first is under ambient light, with the edge of the segment and the bottom bevels of the test plate in focus. The second image is illuminated by a sodium lamp to acquire the interferogram. The interferogram is used to determine the segment surface profile while the ambient image is used to define the lateral scale and offset relative to the edge of the segment.

Custom software allows the user to select the edge of the segment and define a diameter of the test plate in the segment's radial direction. This diameter is transferred to the fringe image, where it is shown as a black line in Figure 5. The software finds the bright and dark fringe centers along this line and assigns steps of  $\frac{1}{2}$  wave in optical path difference (OPD) between adjacent fringe centers. The user can adjust the fringe center positions and must identify local minima and maxima of the OPD, indicated by larger circles in Figure 5, and assign the OPD step between each of these points and the adjacent fringe centers. The user determines the overall sense of the OPD (which regions are high) from the strong astigmatism in the ideal segment surface. The segment has minimum curvature along the parent's radial direction, which runs between about 8:00 and 2:00 in Figure 5.



Figure 4. From left to right, the test plate is placed on the segment edge, the image used for alignment and scaling is taken under ambient light, and the fringe image is taken under a sodium light source with an average wavelength of 589 nm.

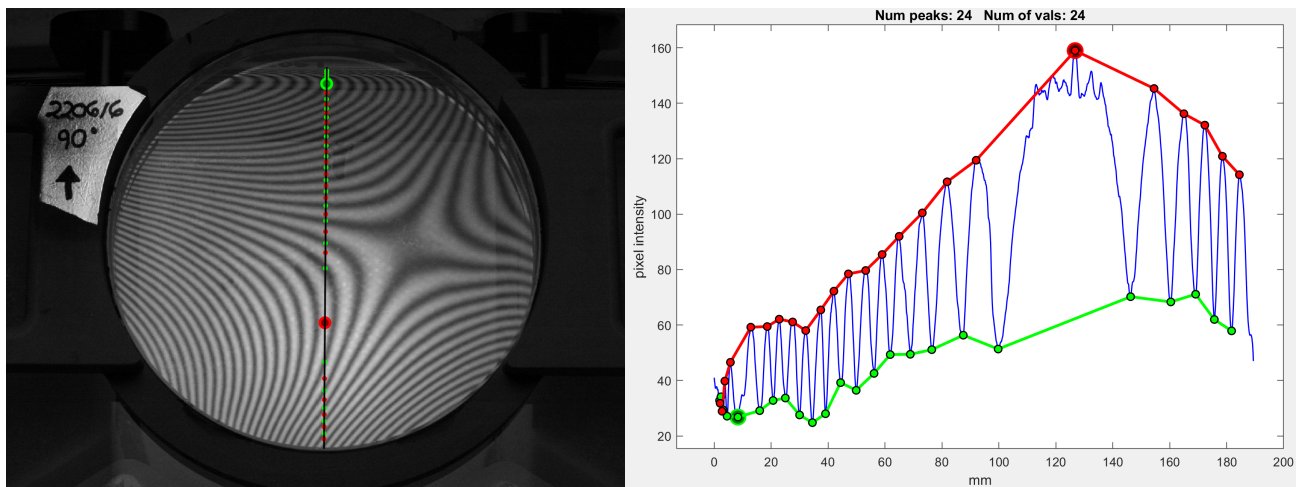


Figure 5. Left: interferogram acquired with the test plate at the edge of Segment 3. Right: intensity along the black line drawn on the interferogram. The edge of the segment is at the top of the interferogram, where the fringes abruptly end. The horizontal axis of the intensity graph indicates distance from the edge.

The raw OPD contains the segment's deviation from the ideal surface (the quantity we want to know) but also the segment's ideal surface, the test plate's ideal spherical surface, and the test plate's deviation from its ideal sphere, along with arbitrary linear terms that depend on how the test plate rests on the segment. We correct for the segment's ideal surface and for the test plate's shape error. To estimate the shape error, we measured 18 well distributed positions at least 0.7 m from the edge, where the segment's figure error is small and varies randomly among the 18 positions. We find a significant shape error equivalent to 110 nm p-v spherical aberration on the test plate's surface. We subtract this test plate error from each measurement of the segment surface.

The quadratic component of OPD is very sensitive to alignment of the black line in Figure 5, and this component is not repeatable. In order to convert the OPD into an accurate measure of the segment's surface error, we adjust the linear and quadratic components of OPD to match those of the full-aperture map over the range  $4.0 \text{ m} < r < 4.15 \text{ m}$  on the segment. The full-aperture measurements are accurate over this range, but have missing data and erroneous data in the outer 5 cm of the finished mirror. At earlier stages of polishing, when slope and curvature errors were larger, the missing and erroneous data could extend further into the clear aperture. The unconstrained part of the test plate OPD, extending beyond  $r = 4.15 \text{ m}$ , is more complete and more accurate than the full-aperture map in this region. Figure 6 shows radial profiles at the edge of Segment 3 at 6 positions, obtained from the full-aperture map and from the adjusted test plate OPD.

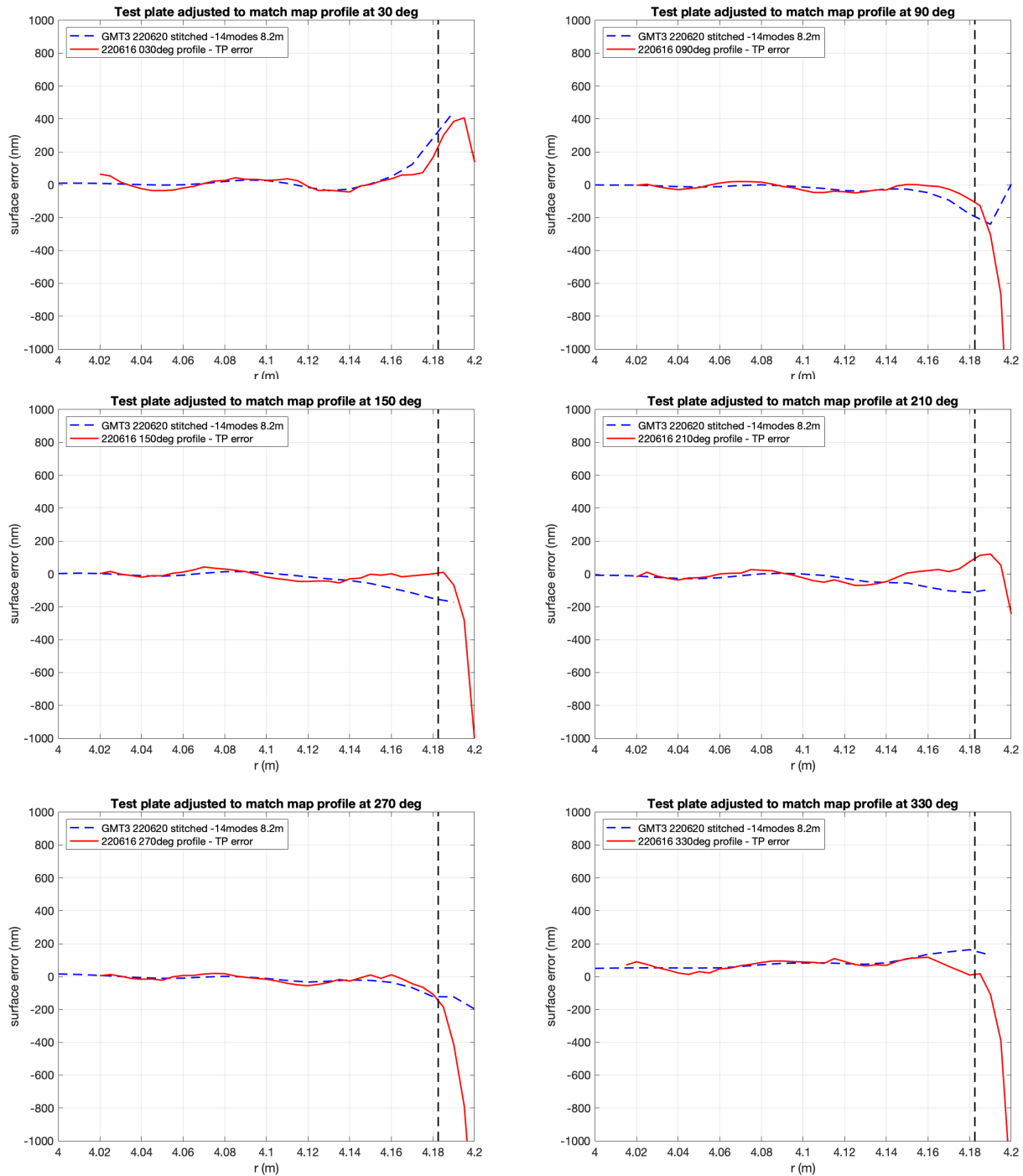


Figure 6. Radial profiles of the segment surface error at the indicated azimuths. Each plot shows the profile given by the full aperture optical tests (blue dashed line) and by the test plate (red solid line). The test plate profile's linear and quadratic terms have been adjusted to match the full-aperture profile over  $r < 4.15$  m. The vertical dashed line marks the edge of the clear aperture. Azimuth =  $0^\circ$  away from the parent vertex and increases counter-clockwise.

### 4.3 Results for Segment 3

Figure 7 shows maps at the completion of Segments 2 and 3. The plots show surface error over the 8.365 m clear aperture, after we simulate the active optics correction that will be made at the telescope. For an off-axis segment, active optics includes alignment (segment displacement) that affects focus, astigmatism and coma, as well as bending with the 165 mirror support actuators. The simulated bending, like the real bending at the telescope, uses a limited number of bending modes, 27 modes for the plots in Figure 7. The allocation of displacement and actuator force for correction of residual manufacturing errors is a small fraction of the full range available to correct errors from all sources at the telescope. Both segments meet the accuracy requirements, including those on the most challenging scales of a few cm. Segment 3 is smoother on small scales but has a little more structure on scales around 1 m. This meter-scale structure, as well as large-scale structure that has been corrected with active optics, is largely limited by repeatability of the full-aperture measurements during the final figuring.

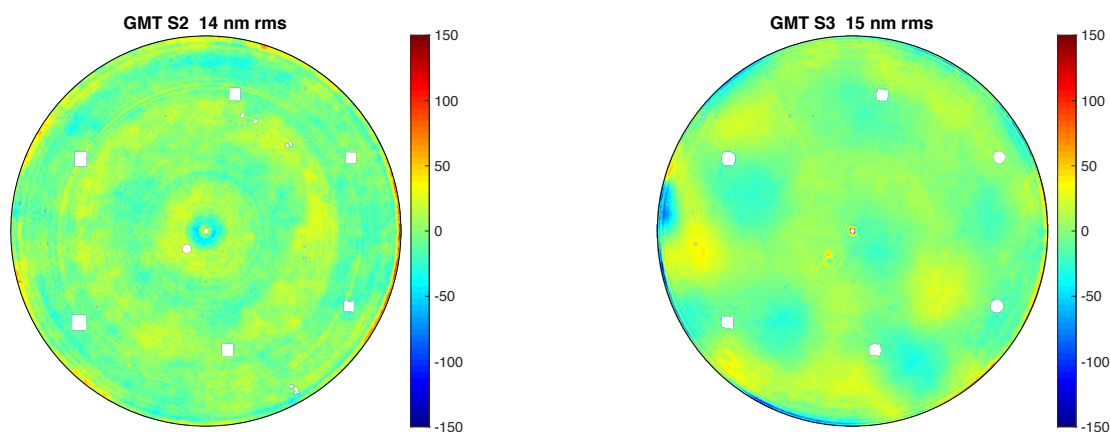


Figure 7. Finished surfaces of GMT Segments 2 and 3. Plots cover the 8.365 m clear aperture and show surface error in nm, after simulated active optics correction using segment alignment and 27 bending modes.

The map of Segment 3 in Figure 7 includes the structure measured with the test plate, but it covers such a narrow annulus at the edge that it can hardly be seen. The detailed structure is clear, however, in the test plate profiles including those shown in Section 4.2. While this structure covers only a small fraction of the clear aperture, it has a significant effect on the structure function. The ability to measure and control this structure was critical to meeting the accuracy requirements.

## 5. CONCLUSION

The Mirror Lab continues to produce primary mirror segments for GMT. The first three off-axis segments are finished and three more segments are in production. Recent achievements include the successful casting of Segment 6 in 2021 and completion of Segment 3 in 2022. We continue to refine polishing and measuring capabilities that are key to efficient production, especially for off-axis segments. We expect to complete all segments on a schedule consistent with the telescope project timeline.

## ACKNOWLEDGMENT

Work for the Giant Magellan Telescope is supported by the GMTO Corporation, an international consortium of leading universities and research institutions representing five countries: Arizona State University, Astronomy Australia Limited, Australian National University, Carnegie Institution for Science, FAPESP–The São Paulo Research Foundation, Harvard University, Korea Astronomy and Space Science Institute, Smithsonian Institution, Texas A&M University, The University of Texas at Austin, University of Arizona, University of Chicago, Weizmann Institute of Science.

## REFERENCES

- [1] J. Fanson, P. J. McCarthy, R. Bernstein, G. Angeli, D. Ashby, B. Bigelow, A. Bouchez, W. Burgett, E. Chauvin, A. Contos, F. Figueroa, P. Gray, F. Groark, R. Laskin, R. Millan-Gabet, A. Rakich, R. Sandoval, M. Pi and N. Wheeler, "Overview and status of the Giant Magellan Telescope project," Proc. SPIE 10700, *Ground-based and Airborne Telescopes VII*, 1070012 (2018).
- [2] James Fanson, Rebecca Bernstein, George Angeli, David Ashby, Bruce Bigelow, Glenn Brossus, Antonin Bouchez, William Burgett, Adam Contos, Richard Demers, Francisco Figueroa, Barbara Fischer, Frank Groark, Robert Laskin, Rafael Millan-Gabet, Marti Pi, Nune Wheeler, "Overview and status of the Giant Magellan Telescope project," Proc. SPIE 11445, *Ground-based and Airborne Telescopes VIII*, 114451F (13 December 2020); doi: 10.1117/12.2561852.
- [3] H. M. Martin, R. Ceragioli, B. Jannuzi, D. W. Kim, J. S. Kingsley, K. Law, A. Loeff, R. D. Lutz, T. J. McMahon, S. Meyen, C. J. Oh, M. T. Tuell, S. N. Weinberger, S. C. West, R. Wortley, "Manufacture of 8.4 m segments for the GMT primary mirror," Proc. SPIE 11451, *Advances in Optical and Mechanical Technologies for Telescopes and Instrumentation IV*, 114514F (13 December 2020); doi: 10.1117/12.2590568.
- [4] J. H. Burge, W. Davison, H. M. Martin and C. Zhao, "Development of surface metrology for the Giant Magellan Telescope primary mirror", Proc. SPIE 7018, *Advanced Optical and Mechanical Technologies in Telescopes and Instrumentation*, 701814 (2008).
- [5] S. C. West, J. H. Burge, B. Cuerden, W. B. Davison, J. Hagen, H. M. Martin, M. T. Tuell and C. Zhao, "Alignment and use of the optical test for the 8.4m off-axis primary mirrors of the Giant Magellan Telescope", Proc. SPIE 7739, *Modern Technologies in Space- and Ground-based Telescopes and Instrumentation*, 77390N (2010).
- [6] R. G. Allen, J. H. Burge, P. Su and H. M. Martin, "Scanning pentaprism test for the GMT 8.4 m off-axis segments", Proc. SPIE 7739, *Modern Technologies in Space- and Ground-based Telescopes and Instrumentation*, 773911 (2010).
- [7] T. L. Zobrist, J. H. Burge and H. M. Martin, "Accuracy of laser tracker measurements of the GMT 8.4 m off-axis mirror segments", Proc. SPIE 7739, *Modern Technologies in Space- and Ground-based Telescopes and Instrumentation*, 77390S (2010).
- [8] P. Su, S. Wang, M. Khreishi, Y. Wang, T. Su, R. E. Parks, P. Zhou, M. Rascon, T. Zobrist, H. Martin and J. H. Burge, "SCOTS: A reverse Hartmann test with high dynamic range for Giant Magellan Telescope primary mirror segments", Proc. SPIE 8450, *Modern Technologies in Space- and Ground-based Telescopes and Instrumentation II*, 84500W (2012).
- [9] B. H. Olbert, J. R. P. Angel, J. M. Hill and S. F. Hinman, "Casting 6.5-meter mirrors for the MMT conversion and Magellan," Proc. SPIE 2199, *Advanced Technology Optical Telescopes V* (1994).
- [10] J. M. Hill, J. R. P. Angel, R. D. Lutz, B. H. Olbert and P. A. Strittmatter, "Casting the first 8.4-m borosilicate honeycomb mirror for the Large Binocular Telescope," Proc. SPIE 3352, *Advanced Technology Optical/IR Telescopes VII* (1998).